kinases and phosphatases

MDPI

Article

Crystallographic Fragment Screening with CK2α′, an Isoform of Human Protein Kinase CK2 Catalytic Subunit, and Its Use to Obtain a CK2α′/Heparin Complex Structure

Christian Werner [1], Tatjana Barthel [2], Hugo Harasimowicz [1], Christelle Marminon [3], Manfred S. Weiss [2], Marc Le Borgne [3] and Karsten Niefind [1,*]

[1] Institute of Biochemistry, Department of Chemistry and Biochemistry, University of Cologne, Zülpicher Str. 47, 50674 Köln, Germany; cwerne17@uni-koeln.de (C.W.); hugo.harasimowicz@gmail.com (H.H.)
[2] Macromolecular Crystallography, Helmholtz-Zentrum Berlin für Materialien und Energie, Albert-Einstein-Str. 15, 12489 Berlin, Germany; tatjana.barthel@helmholtz-berlin.de (T.B.); manfred.weiss@helmholtz-berlin.de (M.S.W.)
[3] Gastroenterology and Technologies for Health Team, Centre de Recherche en Cancérologie de Lyon, Centre Léon Bérard, CNRS 5286, INSERM 1052, Université Claude Bernard Lyon 1, University of Lyon, 69373 Lyon, France; christelle.marminon@univ-lyon1.fr (C.M.); marc.le-borgne@univ-lyon1.de (M.L.B.)
* Correspondence: karsten.niefind@uni-koeln.de; Tel.: +49-221-4706444

Abstract

CK2α and CK2α′, two paralogous members of the human kinome, are catalytic subunits of protein kinase CK2. Together with the regulatory subunit CK2β, they form heterotetrameric holoenzymes. CK2 is the subject of efforts to develop effective and selective inhibitors. For this, secondary binding sites remote from the canonical ATP/GTP cavity are critical. A crystallographic fragment screening with CK2α′ crystals and an established molecular fragment collection was performed to identify new ligands at known or novel sites. It resulted in fourteen CK2α′/fragment structures. Five fragments were found at the CK2β interface of CK2α′ and three fragments at the established αD pocket, which exhibits subtle differences between CK2α and CK2α′; comparative co-crystallisations with CK2α showed that one of them binds to the αD pocket of CK2α′ exclusively. No fragments bound at the substrate-binding region of CK2α′, but a CK2α′ structure with dp10, a decameric section of the substrate-competitive inhibitor heparin, and the indenoindole-type ATP-competitive inhibitor 4w was determined. A comparison with a published CK2α/dp10 structure revealed features consistent with reports about substrate specificity differences between the isoenzymes: dp10 binds to CK2α′ and CK2α with opposite strand orientations, and the local conformations of the isoenzymes in the helix αD region are significantly different.

Keywords: protein kinase CK2; casein kinase 2; human CK2α; human CK2α′; isoenzymes; CSNK2A1; CSNK2A2; crystallographic fragment screening

Academic Editors: Mauro Salvi and Maria Ruzzene

Received: 21 November 2025
Revised: 19 December 2025
Accepted: 29 December 2025
Published: 4 January 2026

1. Introduction

Protein kinase CK2 is a member of the CMGC family of eukaryotic protein kinases [1]. It occurs as a heterotetrameric holoenzyme with a central dimer of regulatory subunits (CK2β) to which two catalytic subunits are attached [2]. In human and other vertebrates, two paralogous isoforms of catalytic CK2 subunits exists, typically called CK2α (product of the gene *CSNK2A1*) and CK2α′ (product of the gene *CSNK2A2*); they have similar sequences; nevertheless, there are subtle differences between CK2α and CK2α′ that are important enough that they cannot fully compensate each other [3,4].

For many years, human CK2 has been a target for the development of inhibitors [5–9], most of them addressing the binding site for the co-substrate, which—as a rare exception among protein kinases—can be ATP or GTP [10]. Due to selectivity problems with ATP/GTP-competitive inhibitors, "jumping-out-of the-catalytic-box" strategies were proposed and pursued [6,11], for which allosteric ligand-binding sites—sometimes called "secondary sites" [12]—remote from the ATP/GTP cavity (the "primary site"; Figure 1a) were required.

One secondary site of CK2α or CK2α′ is the binding interface for CK2β. Small molecules addressing this region are potential protein/protein interaction inhibitors and interfere with the formation of the CK2 holoenzyme. Several peptidic and non-peptidic compounds—among them the cyclic peptidomimetic compound 12 (cpd. 12), visible in Figure 1a—were developed and characterized with respect to their CK2β-antagonistic potential [13–18]. Cpd. 12 was found by high-throughput screening, and it is the only CK2β-antagonistic substance for which a crystal structure in complex with CK2α′ is available (PDB_ID 9FBI).

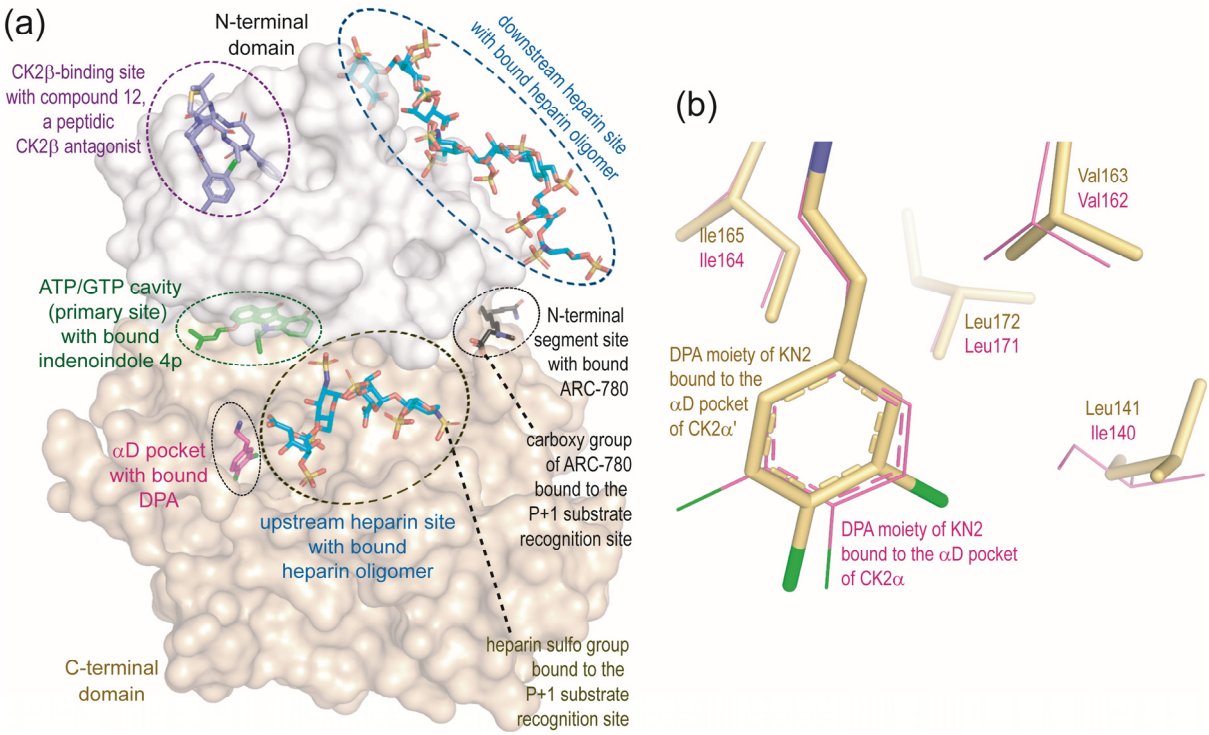

Figure 1. Ligand-binding to primary and secondary sites of CK2α′ and CK2α. (**a**) Surface representation of a CK2α′^{Cys336Ser}/3,4-dichlorophenethylamine (DPA) complex structure [19] (gray: N-terminal domain; yellow: C-terminal domain) with superimposed complex structures of CK2α′^{Cys336Ser}/4p (PDB_ID 7AT9), CK2α′^{Cys336Ser}/ARC-780 (PDB_ID 8Q77), CK2α′^{Cys336Ser}/compound 12 (PDB_ID 9FBI), and CK2α$^{1-335}$/heparin (PDB_IDs 7B8H and 7B8I); for the superimposed complex structures, only the ligands (in the case of ARC-780, only the middle part, which was defined by electron density) were drawn in order to indicate the various binding sites, as indicated in the figure. (**b**) Differences between CK2α′ (yellow C-atoms and bonds) and CK2α (magenta-colored C-atoms and bonds) in the hydrophobic shell of the αD pocket: the side chain difference Leu140/Ile141 correlates with a 180-degree rotation of DPA, the αD pocket anchor group of the bivalent inhibitor KN2 [19]. The figure was prepared with PyMOL, version 1.7.0.3 [20].

Another allosteric ligand-binding site is the αD pocket, which is located adjacent to the ATP/GTP cavity. It is a "cryptic" site [21] because it is normally blocked by side chains from the nearby helix αD and accessible only after its opening in the presence of a suitable ligand. The αD pocket was discovered by fragment screening with human CK2α

crystals and exploited to construct a highly selective bivalent CK2 inhibitor addressing the ATP/GTP site and the αD pocket itself in parallel [22,23]. Later, an αD pocket was observed in the isoenzyme CK2α′ as well, occupied by 3,4-dichlorophenylethylamine (DPA) [19]. DPA, one of the molecular fragments identified via screening with CK2α crystals [22], had been soaked into crystals of CK2α′^{Cys336Ser}, which is an oxidation-insensitive CK2α′ variant [19]. It was then used as αD pocket anchor group of KN2 (Figure 1b), a second bivalent CK2 inhibitor with excellent inhibition and selectivity properties [19]. Meanwhile, further highly potent and selective bivalent CK2 inhibitors binding both to the ATP/GTP cavity and to the αD pocket have been published [24–27].

In the context of the bivalent inhibitor KN2, it was noted that in complex structures with either CK2α or CK2α′, the DPA part of KN2 (Figure 1b) is orientated differently: bound to the αD pocket of CK2α, the chloro substituent in *meta* position points outwards in the direction of the dismantled helix αD; in complex with CK2α′, however, the dichlorophenyl moiety is rotated by 180°, so that the *meta*-chloro substituent is in contact with the hydrophobic core residue Leu141 (Figure 1b). The CK2α equivalent of this residue is Ile140, whose space requirements and rigidity may prevent the *meta*-chloro substituent from being in its direct proximity. This finding has been speculated to be exploitable for generating isoenzyme-selective CK2 inhibitors [19]. In fact, KDX1381, a recently described bivalent CK2 inhibitor, has a significant preference for CK2α compared to CK2α′ [25].

A further secondary binding site was discovered so far only in CK2α′, namely by extensively soaking and desalting of CK2α′^{Cys336Ser} crystals with ARC-780. This is a compound originally designed to be a bisubstrate inhibitor, meaning that it simultaneously addresses the ATP/GTP site and the binding region for protein and peptide substrates [28]. Surprisingly, however, two copies of ARC-780 were found in a complex structure with CK2α′^{Cys336Ser}, one at the ATP/GTP cavity and the other—partly visible in Figure 1a—at a novel "N-terminal segment site" that overlaps with the P+1 recognition site of protein/peptide substrates [28].

The substrate recognition area—also the binding region of heparin [29,30], one of the oldest known CK2 inhibitors [31,32]—can also be classified as a secondary site. CK2 is an acidophilic protein kinase with the consensus sequence S/T-E/D-X-E/D for substrate recognition [33] (however, with interesting variations in substrate recognition between CK2α and CK2α′ [3,34]). Its specific interactions with anionic substrates or substrate-competitive inhibitors are dominated by ionic forces, which are weakened by the high salt concentrations often used in crystallization and soaking media. In addition, divalent anions, as sometimes found in the substrate recognition region of CK2 structures [2,28,35], compete specifically with those interactions. Therefore, the only CK2 co-crystal structures with higher-molecular-weight ligands bound in the substrate recognition region are the above-mentioned CK2α′^{Cys336Ser}/ARC-780 complex structure [28] and two CK2α$^{1\text{-}335}$ structures in complex with a heparin decasaccharide [30]. This heparin fragment binds at two different locations of CK2α, namely to a part of the P+1 recognition region of the substrate-binding site (Figure 1a) and to a polybasic stretch at the beginning of the long helix αC, the only helical element of the N-terminal domain, where acidic substrate side chains downstream of the P+3 substrate recognition site are accommodated (Figure 1a) [30].

Finally, a further allosteric site was recently postulated to be located in the C-terminal domain of CK2α′ [36]. However, a structural confirmation of this assumption was not provided so far.

The study presented here was inspired by the question of whether crystallographic fragment screening, which had previously been performed only with CK2α [22,23], can also provide a deeper understanding of the binding potential of the known binding sites or even uncover novel binding sites in the case of CK2α′. From a methodological point

of view, it was based on the availability of robust CK2α′^{Cys336Ser} crystals with excellent X-ray diffraction properties on the one hand [28,37], and, on the other hand, on the well established and continuously developed platform for crystallographic fragment screening at the Helmholtz Centre Berlin (HZB) [38–41].

Against the background of the difference between CK2α and CK2α′ in the binding of KN2 at the αD pocket (Figure 1b), a particular aim of this screening study was to find new fragments binding to the αD pocket of CK2α′ and to subsequently check if they can occupy the αD pocket of CK2α as well.

Differences between CK2α and CK2α′ have also been reported for substrate recognition [3,34]. Even before the crystallographic fragment screening, we had started efforts to uncover structural reasons for this and to create a structural basis for the development of isoenzyme-specific bisubstrate inhibitors. In this context, crystallographic fragment screening provided helpful methodological input for the elucidation of a CK2α′^{Cys336Ser} structure in complex with the substrate-competitive inhibitor heparin [29,31], which was then used for a comparison with published CK2α$^{1-335}$/heparin structures [30], as explained below.

2. Results and Discussion

2.1. Crystallographic Fragment Screening with CK2α′^{Cys336Ser} Crystals

2.1.1. Overview of the Fragment Screening Results

An established protocol to grow triclinic well-diffracting CK2α′^{Cys336Ser} crystals [28,37] was optimized by using the tight-binding ATP-competitive CX-4945 [8] as a crystallization chaperone, which made the procedure faster, more reliable, and more efficient. This allowed the preparation of more than 300 crystals of suitable size (50 to 150 µm in each direction) within one month. The fact that the ATP/GTP binding site of the crystalline CK2α′^{Cys336Ser} was occupied by the high-affinity CK2 inhibitor CX-4945 was not a problem, but even welcome, because we were primarily interested in ligands binding to secondary sites.

Each of the 96 compounds of the F2X-Entry screen [38] was soaked for 24 h at a maximum concentration of 100 mM into at least two CK2α′^{Cys336Ser}/CX-4945 crystals. In parallel with the soaking with fragments, the crystals were dehydrated as described in detail in the Materials and Methods section. This significantly reduced the handling time because it enabled direct flash-freezing of harvested crystals in liquid nitrogen after soaking.

For six fragments, soaking caused the CK2α′^{Cys336Ser} crystals to completely lose their X-ray diffraction capability. In the other 90 cases, however, X-ray diffraction data were collected, processed, and used for structure determination. Fourteen members of the F2X-Entry screen [38] (Table 1) were found to bind to the enzyme as ligands, corresponding to a hit rate of 14.6%. The high-resolution limit of the 14 refined crystal structures ranges from 1.660 Å to 0.892 Å (Table S1). The ligands bind to three established binding sites (ATP/GTP cavity, αD pocket, CK2β binding site) and to three novel sites referred to as "further site" in Table 1. These further sites will not be illustrated and discussed here, because two of them—found for D10 and F08—are most likely crystal-packing artifacts, and in one case (E11), the further site is poorly occupied and located so far from functionally critical regions of the enzyme that its exploitation for the design of bivalent ligand is improbable.

Strictly speaking, there were even a few more hits in which the electron density in the ATP/GTP cavity indicated binding of a fragment. However, these were ligands that did not completely displace CX-4945 from its site, which led to overlapping electron densities and refinement problems. Since we were not primarily interested in new ligands of the ATP/GTP cavity, we did not proceed with such problematic hits.

Table 1. Compounds of the F2X-Entry screen [38] identified as ligands of CK2α′^{Cys336Ser} by crystallographic fragment screening.

F2X-Entry Screen ID	Fragment Structure SMILES Notation	Binding Site(s) to CK2α′	PDB_ID of CK2α′^{Cys336Ser}/ CK2α$^{1-335}$ Complex
C02	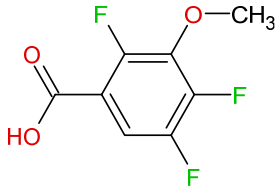 Fc1cc(C(=O)O)c(F)c(OC)c1F	ATP/GTP cavity αD pocket	9IHG/9HXU
C06	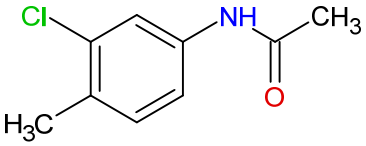 CC(=O)Nc1cc(Cl)c(C)cc1	CK2β interface	9Q9A/---
C07	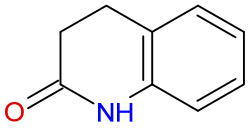 O=C1CCc2ccccc2N1	CK2β interface	9Q9B/---
D02	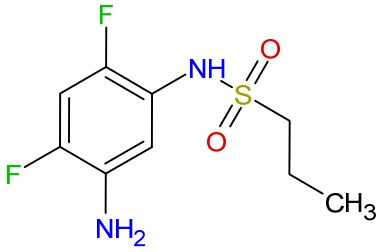 O=S(=O)(CCC)Nc1cc(N)c(F)cc1F	αD pocket	9IHI/9HYH
D04	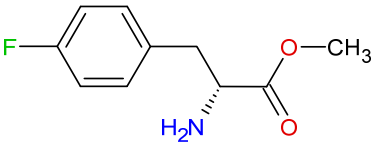 O=C(OC)[C@H](N)Cc1ccc(F)cc1	ATP/GTP cavity	9Q9C/---
D06	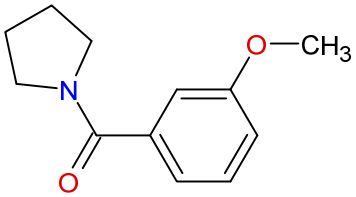 O=C(N1CCCC1)c1cc(ccc1)OC	CK2β interface	9Q9D/---
D10	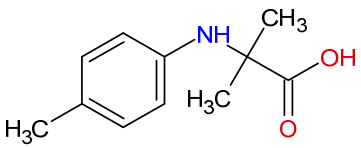 CC(C)(Nc1ccc(C)cc1)C(=O)O	ATP/GTP cavity further site	9Q9G/---

Table 1. *Cont.*

F2X-Entry Screen ID	Fragment Structure SMILES Notation	Binding Site(s) to CK2α′	PDB_ID of CK2α′^{Cys336Ser}/ CK2α$^{1-335}$ Complex
E03	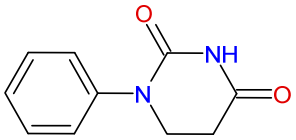 O=C1NC(=O)CCN1c1ccccc1	ATP/GTP cavity	9Q8Q/---
E11	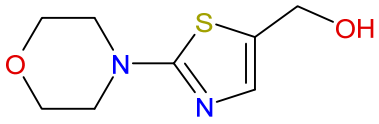 OCc1cnc(s1)N1CCOCC1	CK2β interface further site	9QAB/---
F02	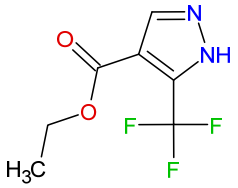 FC(F)(F)c1n[NH]cc1C(=O)OCC	ATP/GTP cavity αD pocket	9Q8C/9HZH
F08	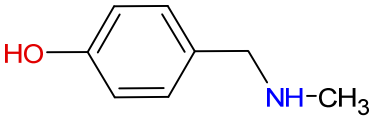 Oc1ccc(CNC)cc1	Further site	9QAG/---
G07	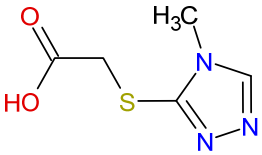 OC(=O)CSc1nncn1C	ATP/GTP cavity	9QAK/---
H02	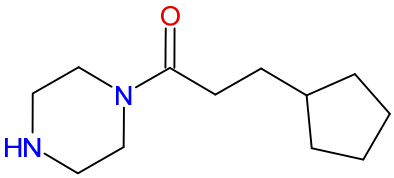 O=C(CCC1CCCC1)N1CCNCC1	CK2β interface	9QB6/---
H07	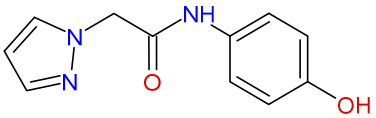 O=C(Cn1cccn1)Nc1ccc(O)cc1	ATP/GTP cavity	9QB0/---

2.1.2. Fragments Occupying the ATP/GTP Binding Site of CK2α′

Seven fragments of the F2X-Entry screen [38] were found as ligands at the ATP/GTP binding site (Table 1, Figure 2), two of them—D10 (Figure 2c) and F02 (Figure 2e)—even more than once. This was surprising because this site was blocked before soaking byCX-4945, known to be a tight-binding inhibitor, as shown in the case of CK2α [42], but obviously the large fragment concentration (up to 100 mM) could counteract this high affinity.

Looking at the seven ligands as a whole, they cover all known subsites of the ATP/GTP cavity: some of the fragments (E03 in Figure 2d, H07 in Figure 2g) address the backbone

of the interdomain hinge, while all others bind to deeper docking anchors such as Lys69, Phe114, or Asp176. In the case of E03, the break in the electron density in the 1,3-diazinane ring, which can be seen in Figure 2d, is surprising. Possible explanations for this include ring opening or rapid local conformational changes in the non-planar ring system, but the true reason remains unclear.

Despite popular "jumping-out-the-catalytic-box" strategies [11], the development of ATP-competitive compounds is still an actual field of CK2 inhibitor development [43], and the fact that an ATP-competitive classic such as CX-4945 is also applicable beyond tumor therapy was only recently demonstrated for CK2-associated obesity [44]. The future will show whether some of the fragment identified here as ligands in the ATP/GTP binding pocket—possibly integrated as substructures into larger inhibitors via Frag4Lead [40] or comparable workflows—have similar application potentials.

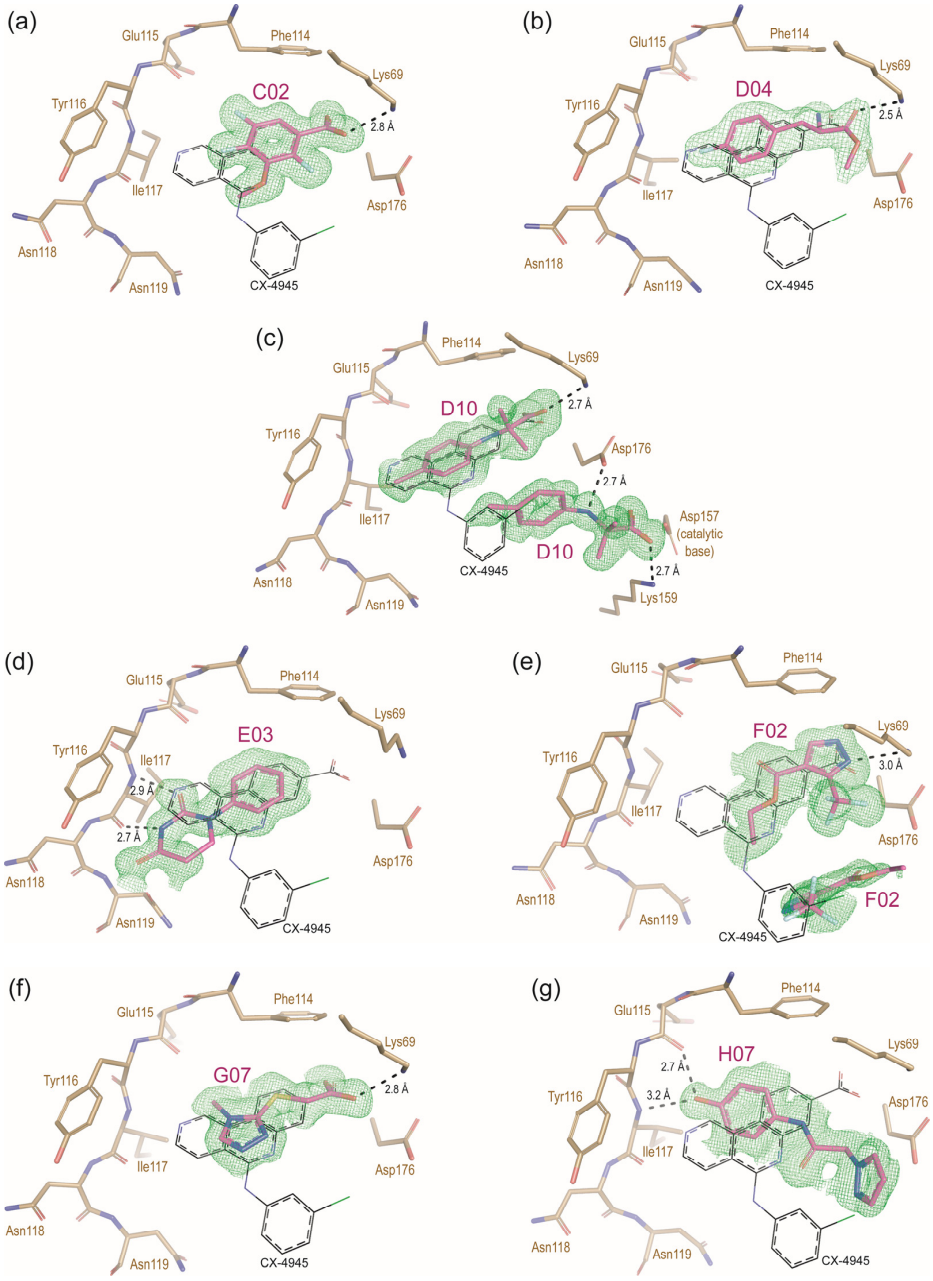

Figure 2. ATP/GTP binding cavity in structures of CK2α′^{Cys336Ser} in complex with various F2X-Entry screen fragments [38]: C02 (**a**), D04 (**b**), D10 (**c**), E03 (**d**), F02 (**e**), G07 (**f**) and H07 (**g**). The respective

fragments were drawn with magenta-colored C-atoms and are covered by final 2Fo-Fc electron density (green mesh) with a cutoff level of 1.0 σ. CX-4945 from PDB_ID 6HMB (black C-atoms) was drawn for comparison after structural overlay. Critical H-bonds are indicated with dashed lines. The figure was prepared with PyMOL, version 1.7.0.3 [20]. A supplementary version of the figure with Fo-Fc OMIT maps (cutoff level: 4.0 σ) instead of 2Fo-Fc electron density maps is available online in the Supporting Material (Figure S1).

Fragment D10 [2-methyl-2-(4-methylanilino) propanoic acid] (Figure 2c) deserves a special note, because a second, well defined copy of this fragment is bound in the ATP/GTP binding site region. This second D10 ligand protrudes deeply into the core of the active site around the catalytic base Asp157 (Figure 2c), i.e., into an area that, in a phosphorylation reaction, is required for the substrate side chain to be phosphorylated. One could therefore imagine that connecting the two D10 ligands shown in Figure 2c with a suitable chemical linker could lead to a novel class of CK2 bisubstrate inhibitors.

2.1.3. Fragments Binding in the CK2β Interface Region of CK2α′

The five fragments C06, C07, D06, E11, and H02 (Table 1) were observed at the CK2β interface region in the vicinity of Leu42 and Phe55 (Figure 3). These two residues are equivalent to the CK2α residues Leu41 and Phe54, which had been identified as hot spots of the CK2α/CK2β interaction [45]. On the side of CK2β, the interaction hot spots are Tyr188 and Phe190; they were preserved by Laudet et al. [13] when they designed the cyclic CK2β-antagonistic peptide Pc from the CK2α-binding region of CK2β. Later, a structure analysis disclosed that Pc binds to CK2α in fact exactly like the equivalent part of its mother protein CK2β [18]. Superimposing this CK2α/Pc structure (PDB_ID 4IB5) onto each of the five CK2α′^{Cys336Ser}/fragment structures demonstrates that the bound F2X-Entry screen fragments overlap with the Tyr188 side chain of Pc, as exemplarily illustrated for the CK2α′^{Cys336Ser}/C06 structure in Figure 3a.

In contrast, the five F2X entry screen fragments do not overlap with the cyclic peptidomimetic cpd. 12, as shown by 3D fits with the complex structure CK2α′^{Cys336Ser}/cpd. 12 (PDB_ID 9FBI) (Figure 3b–f). Cpd. 12 addresses the binding region of Phe190, but not that of Tyr188, as can be seen by comparing Figure 3a with Figure 3b. This opens the idea of optimizing cpd. 12 in its CK2β-antagonistic effect by linking it to one of the fragments overlapping with Tyr188.

These structural comparisons show that the CK2β interface is a fairly extended binding region rather than a small cavity. Accordingly, the risk that it is incorporated into crystal contacts and altered in its binding potential is relatively high. In fact, all five F2X-Entry screen fragments shown in Figure 3 are also in contact with a symmetry-equivalent CK2α′^{Cys336Ser} protomer. While it is therefore uncertain whether they also bind to CK2α′ in the non-crystalline state, the five fragments may nevertheless have the potential to be used as starting points for the design of new CK2β antagonistic compounds or to optimize existing ones [14–17]. Thus, these F2X screen fragments effectively enrich the existing knowledge about the chemical space of CK2β interface ligands.

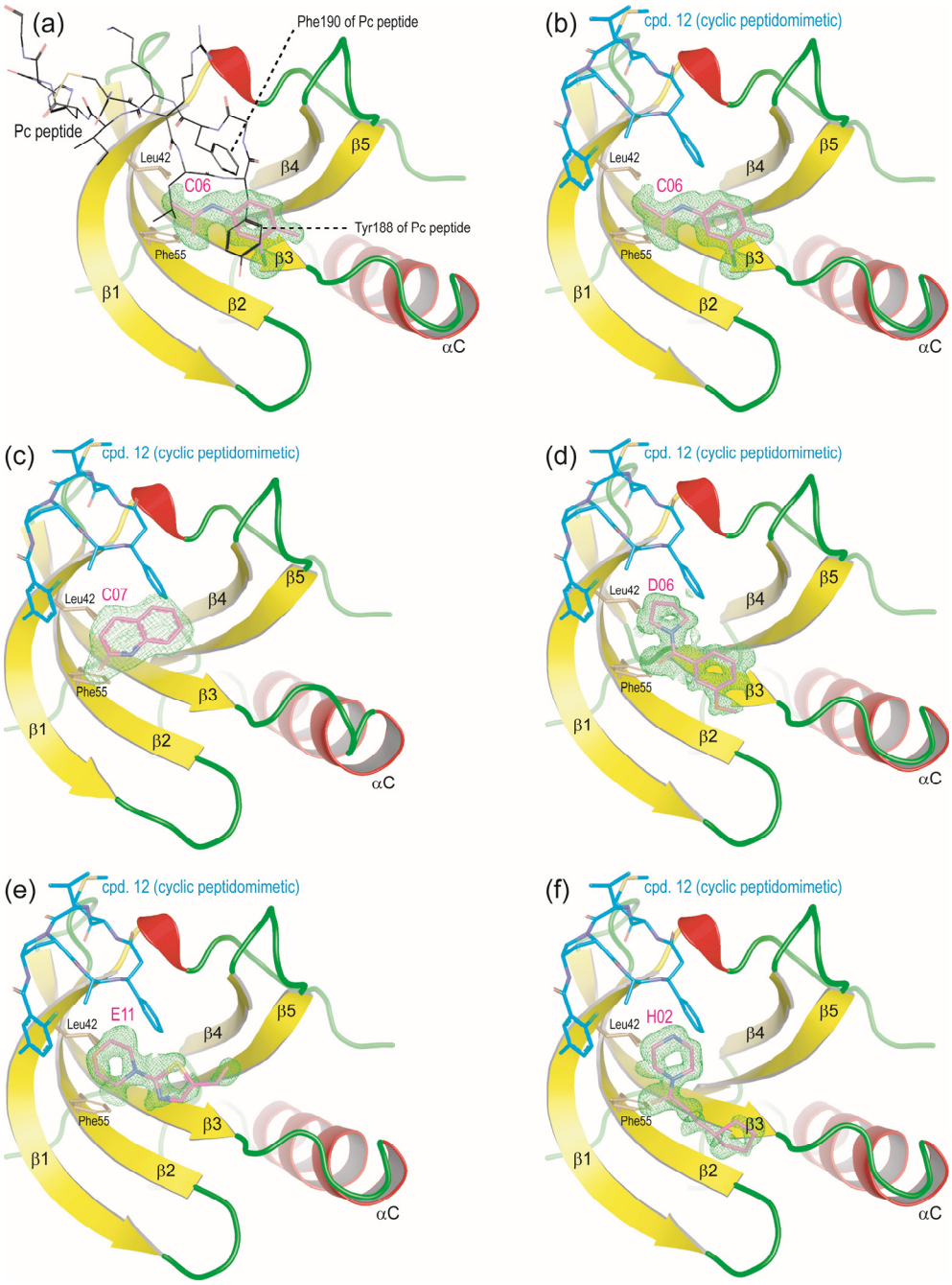

Figure 3. F2X-Entry fragments identified at the CK2β interface region of CK2α′^{Cys336Ser}. In each of the pictures, the N-terminal domain of CK2α′^{Cys336Ser} is displayed together with the bound fragment, which is depicted with magenta-colored C-atoms and covered with final 2Fo-Fc electron density drawn as a green mesh with a cutoff level of 1.0 σ. (**a**) The cyclic peptide Pc was drawn with black C-atoms after superimposition of the CK2α$^{1-335}$/Pc structure [18] (PDB_ID 4IB5) on the CK2α′^{Cys336Ser}/C06 structure. (**b**–**f**) The cyclic CK2β-antagonistic and peptidomimetic cpd. 12 was drawn with cyan-colored C-atoms after superimposition of the CK2α′^{Cys336Ser}/cpd. 12 structure (PDB_ID 9FBI) on the CK2α′^{Cys336Ser} structures in complex with the fragments C06 (part (**b**)), C07 (part (**c**)), D06 (part (**d**)), E11 (part (**e**)) and H02 (part (**f**)). The figure was prepared with PyMOL, version 1.7.0.3 [20]. A supplementary version of the figure with Fo-Fc OMIT maps (cutoff level: 4.0 σ) instead of 2Fo-Fc electron density maps is available online in the Supporting Material (Figure S2).

2.1.4. Fragments Occupying the αD Pocket

The fragments C02, D02, and F02 of the F2X-Entry screen [38] were found as ligands at the αD pocket of CK2α′^{Cys336Ser} (Figure 4). While D02 (Figure 4a) and C02 (Figure 4e)

are well defined by electron density, this is not the case for F02 (Figure 4c), which could be identified as an αD pocket ligand only by PanDDA [46] and which has a low occupancy (0.43) in the refined complex structure. These hits are particularly interesting because C02, D02, and F02 have not been described so far as αD pocket ligands for the isoenzyme CK2α. As illustrated in Figure 1b, there are subtle differences between the paralogs CK2α and CK2α′ at the αD pocket, which might be exploited for the development of isoenzyme-specific inhibitors.

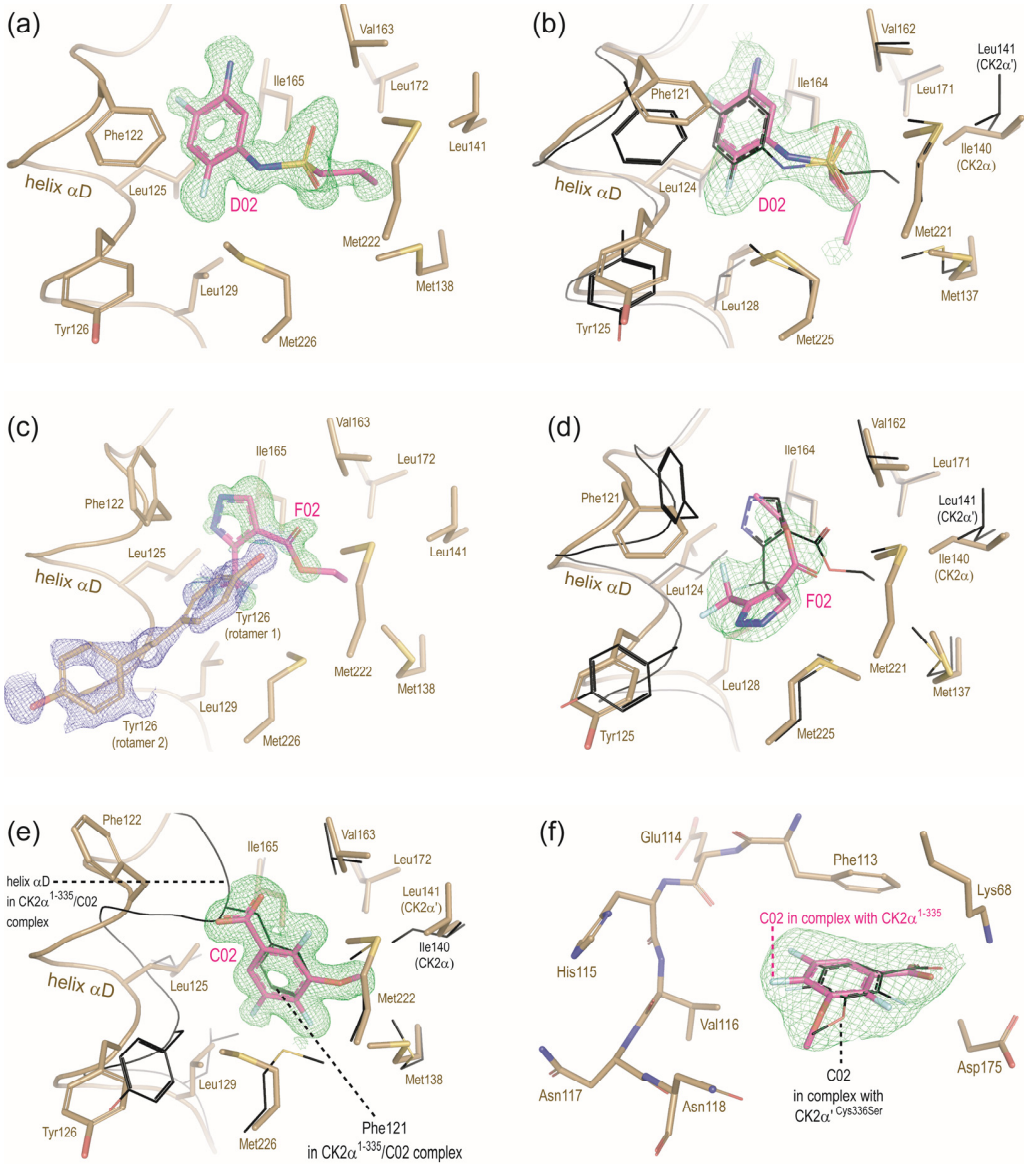

Figure 4. Fragments of the F2X-Entry screen [38] binding to the αD pocket of CK2α′^{Cys336Ser}. (**a**) Fragment D02 in the αD pocket of CK2α′^{Cys336Ser}. (**b**) Fragment D02 in the αD pocket of CK2α$^{1-335}$; for comparison, the equivalent part of the CK2α′^{Cys336Ser}/D02 complex structure was drawn with black C-atoms. (**c**) Fragment F02 in the αD pocket of CK2α′^{Cys336Ser}. (**d**) Fragment F02 in the αD pocket of CK2α$^{1-335}$; for comparison, the equivalent part of the CK2α′^{Cys336Ser}/F02 complex structure was drawn with black C-atoms. (**e**) Fragment C02 in the αD pocket of CK2α′^{Cys336Ser}; for comparison, the equivalent part of the CK2α$^{1-335}$/C02 complex structure was drawn with black C-atoms. (**f**) Fragment C02 at the ATP/GTP cavity of CK2α$^{1-335}$; for comparison, C02 as bound to the ATP/GTP cavity of

CK2α′^{Cys336Ser} (visible also in Figure 2a) was drawn with black C-atoms. Pieces of final 2Fo-Fc electron density around the bound ligands (green) and additionally around Tyr126 in part (**c**) (blue) were depicted with a cutoff level of 0.9 σ. The main fragments, to which the electron densities refer, were depicted with magenta-colored C-atoms. The labeling refers CK2α′^{Cys336Ser} in parts (**a**,**c**,**e**) and to CK2α$^{1-335}$ in parts (**b**,**d**,**f**), if not explicitly stated otherwise. The picture was prepared with PyMOL, version 1.7.0.3 [20]. A supplementary version of the figure with Fo-Fc OMIT maps instead of 2Fo-Fc electron density maps is available online in the Supporting Material (Figure S3).

For this, it would be favorable if C02, D02, and F02 did not bind to the αD pocket of CK2α, or at least bound significantly worse than to that of CK2α′. We tested this crystallographically: although not a suitable method to determine binding affinities between proteins and ligands quantitatively, crystallography can provide a qualitative impression of differences in binding strength. CK2α$^{1-335}$, a C-terminally truncated version of human CK2α that is fully active and well established for crystallographic purposes [47], was applied for this comparative crystallographic investigation.

CK2α$^{1-335}$ was crystallized after pre-incubation with both 0.5 mM CX-4945 and 100 mM of either C02, D02, or F02, i.e., under similar ligand concentrations used before for soaking of CK2α′^{Cys336Ser} crystals with fragments of the F2X-Entry screen [38]. In the case of the combination D02/CX-4945, the ATP/GTP cavity of CK2α$^{1-335}$ harbors CX-4945, while fragment D02 binds to the αD pocket, with the only difference from CK2α′^{Cys336Ser}-bound D02 being that the terminal propyl group of the propylsulfonamide substituent is turned away from the nearby side chain (Ile140 in CK2α, but Leu141 in CK2α′) (Figure 4b). This minor conformational difference is apparently not sufficient to generate a significant affinity gap. Nevertheless, the example of D02 emphasizes that a spatial constraint is imposed by the side chain of Ile140 in the posterior region of the αD pocket of CK2α. Compounds that can evade this constraint by adjusting their conformation—such as KN2 (Figure 1b) or D02 (Figure 4b)—can still bind.

Another possible adaptation of a ligand to the paralog-specific local constraints within the αD pocket is the adjustment of the orientation of the whole molecule. This can be seen from fragment F02: its orientation in the αD pocket of the CK2α$^{1-335}$/F02 complex (which likewise contains CX-4945 in the ATP/GTP cavity) is so different from that in the CK2α′^{Cys336Ser}/F02 complex that the two central pyrazole rings do not overlap in structural overlay (Figure 4d). A further difference between the F02 complex structures of the two isoenzymes is that the F02 ligand in the αD pocket of CK2α$^{1-335}$ is well defined by electron density (in both CK2α$^{1-335}$ protomers of the asymmetric unit) (Figure 4d), while in the αD pocket of CK2α′^{Cys336Ser} (Figure 4c), it is only partially recognizable, namely as an alternative (with an occupancy factor of 0.43) to the side chain of Tyr126, which itself occurs in two alternative conformations; correspondingly, the electron density around F02 is weaker and somewhat diffuse here. Given the fact that the CK2α′^{Cys336Ser}/F02 structure contains a well defined F02 ligand at the ATP/GTP cavity (Figure 2e, Figure S1e), it is especially remarkable that its αD pocket is only partially filled with F02, whereas that of CK2α$^{1-335}$ is completely occupied. This difference seems to indicate that the αD pocket of CK2α may be better suited for binding of F02 than that of CK2α′.

In the case of fragment C02, it is the other way around: while C02 is clearly defined by electron density in the αD pocket of CK2α′^{Cys336Ser}, it is not visible at all in the αD pocket of CK2α$^{1-335}$, which is instead occupied by the side chain of the helix αD residue Phe121 (Figure 4e). C02 is the most sterically demanding of the fragments we could identify as CK2α′ ligands (Table 1), since it is the only one with five substituents attached to the central ring system. The mutual adaptability of C02, on the one side, and of the αD pocket of CK2α, on the other side, is possibly not sufficient to accommodate such a bulky molecule.

Remarkably, this striking difference between CK2$\alpha^{1\text{-}335}$ and CK2$\alpha'^{Cys336Ser}$ in the binding of fragment C02 is restricted to the αD pocket. While the latter is free from C02 in the CK2$\alpha^{1\text{-}335}$/C02 complex structure (structure with black C-atoms in Figure 4e), the ATP/GTP cavity of this structure harbors C02, which is well defined by electron density in spite of the presence of CX-4945 during co-crystallization (Figure 4f). This represents a kind of internal control for the significance of the observed affinity difference at the αD pocket. Overall, this analysis suggests that C02 is a top candidate for the anchor group of a bivalent compound that inhibits CK2α′ significantly better than CK2α. The reverse—better inhibition of CK2α over CK2α′—might be achieved with F02 as an αD pocket warhead, albeit this conclusion is less clear from this crystallographic comparison.

2.2. Characterization of the CK2α′ Substrate-Binding Site by a Complex Structure with Heparin

None of the F2X-Entry screen fragments [38] was bound in the region of the substrate-binding site of CK2$\alpha'^{Cys336Ser}$. The region is dominated by positively charged residues, which requires anionic counterparts for binding. Although anionic fragments are present in the F2X-Entry screen, the lack of hits was not surprising, because the salt concentration during soaking was so high (900 mM LiCl, 200 mM Tris/HCl) that ionic interactions could only be effective in shielded areas (such as the inner side of the ATP/GTP cavity facing away from the surface).

Nevertheless, the experimental approach used in crystallographic fragment screening, specifically exposing CK2$\alpha'^{Cys336Ser}$ crystals to the highest possible ligand concentration during soaking, was one of two critical methodological factors enabling the achievement of a long-standing goal, namely the elucidation of the structure of CK2$\alpha'^{Cys336Ser}$ in complex with dp10, a decameric fragment of the anionic substrate-competitive CK2 inhibitor heparin (Figure 5a), and with the indenoindole-like ATP/GTP-competitive inhibitor 4w [48] (Figure 5b), intended to serve as an ATP/GTP cavity warhead of a prospective bisubstrate inhibitor. The second key measure was to reduce the salt concentration as much as possible, an approach that had been successfully applied to discover the "upstream heparin-binding site" of CK2$\alpha^{1\text{-}335}$ [30] and the "N-terminal segment site" of CK2$\alpha'^{Cys336Ser}$ [28], both indicated in Figure 1a.

For CK2$\alpha^{1\text{-}335}$, upstream and downstream heparin-binding regions—named according to their location relative to the phosphorylation position in a CK2 substrate—were identified by co-crystallization with dp10 [30] (Figure 1a). In the CK2$\alpha'^{Cys336Ser}$/4w crystals used here for extensive soaking with dp10, both heparin-binding sites were accessible and not blocked by crystal contacts; nevertheless, dp10 (more precisely, a part of it) was found exclusively at the upstream binding site (Figure 5c). One disaccharide consisting of N,O6-α-*D*-disulfoglucosamine (SGN) and 2-sulfo-α-*L*-iduronic acid (IDS) (Figure 5a) is well defined by electron density, while the subsequent residue SGN3 is only partially visible (Figure 5f).

In both CK2α isoenzymes, the P+1 loop (CK2α: Arg191 to Glu201; CK2α′: Arg192 to Glu202) and the catalytic loop (CK2α: Arg155 to Asn161; CK2α′: Arg156 to Asn162) provide the most critical side chains for binding of heparin at the upstream site (Figure 5d,e), which is primarily mediated by hydrogen bonds and ionic interactions (Figure 5f). In particular, Lys159 and His161 in CK2α′ (respectively, their CK2α equivalents Lys158 and His160) from the core region of the active site are key residues for heparin-binding.

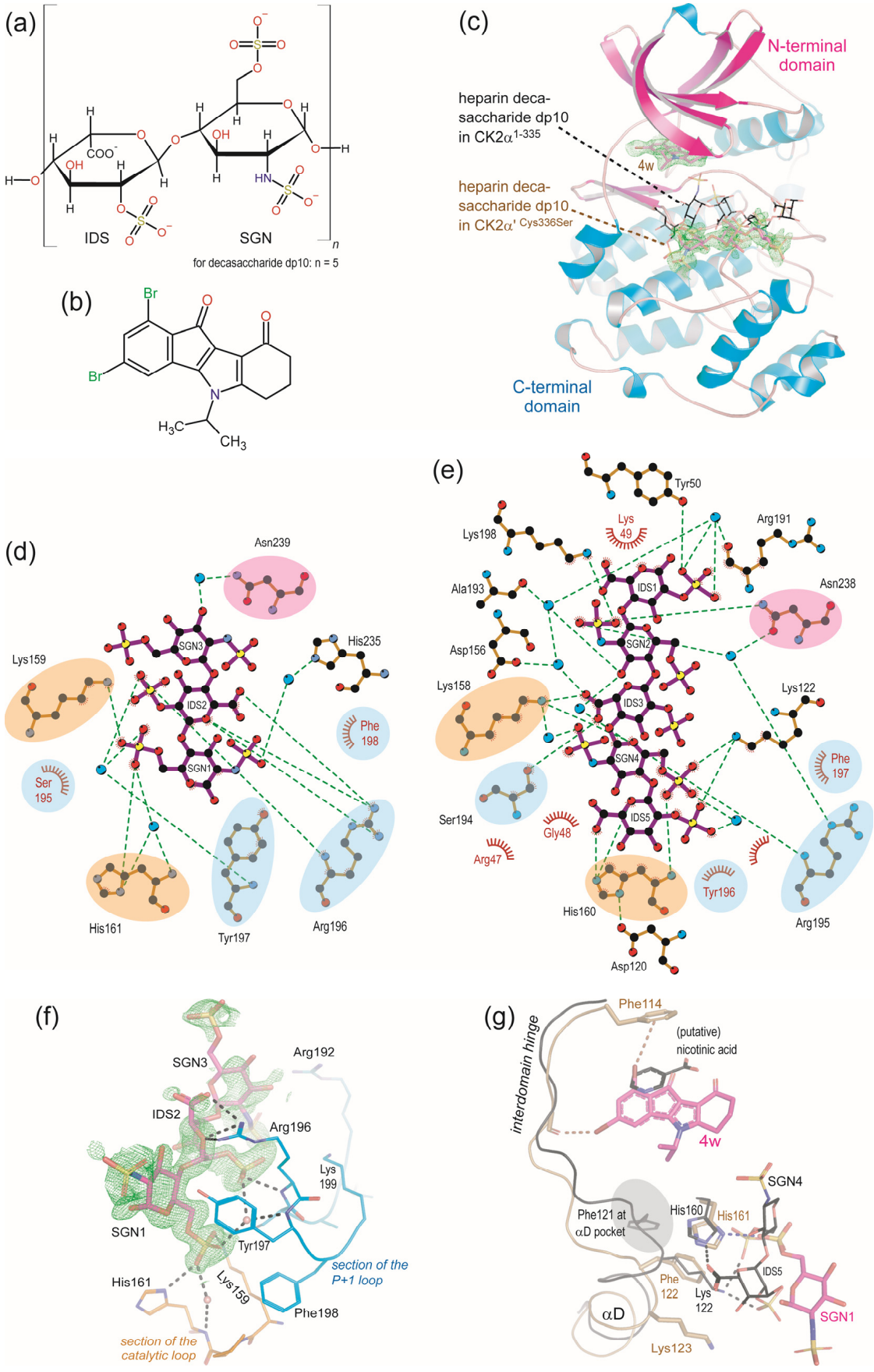

Figure 5. Heparin-binding to CK2α′^{Cys336Ser} and to CK2α$^{1-335}$ [30] (PDB_ID 7B8H) in comparison. (**a**) A repetitive unit of heparin consisting of N,O6-α-*D*-disulfoglucosamine (SGN) and 2-sulfo-α-*L*-iduronic acid (IDS). (**b**) The indenoindole-type CK2 inhibitor 4w [48]. (**c**) Structural overview of the

CK2α′^{Cys336Ser}/4w/dp10 complex; the two ligands are drawn with magenta-colored C-atoms and covered with final 2Fo-Fc electron density (green mesh; contouring level: 1 σ); for comparison, dp10 as bound to CK2α$^{1-335}$ was drawn with black C-atoms after 3D fitting. (**d**,**e**) Comparative 2D plots of dp10 binding to CK2α′^{Cys336Ser} (picture (**d**)) and to CK2α$^{1-335}$ (picture (**e**)) generated with LigPlot [49]; equivalent residues contributing to dp10 binding in both isoenzymes are highlighted with background of different colors (blue: P+1 loop, orange: catalytic loop, and magenta: other regions); hydrogen bonds are indicated by green dashed lines. (**f**) Binding of dp10 to CK2α′^{Cys336Ser}: involvement of the P+1 loop (light blue C-atoms) and the catalytic loop; hydrogen bonds are indicated by gray dashed lines; dp10 is covered by electron density (green mesh; contouring level: 1 σ). (**g**) Involvement of the helix αD in heparin-binding depending on the local conformation of the interdomain hinge/helix αD region; the picture shows a structural comparison between the CK2α′^{Cys336Ser}/dp10/4w complex (colored C-atoms and colored labels for residues) and the CK2α$^{1-335}$/dp10 complex (black C-atoms and black labels for residues), which in addition contains a small ligand (presumably nicotinic acid; drawn with black C-atoms) at the ATP/GTP cavity; dashed lines indicate either halogen bonds of 4w or hydrogen bonds. Parts (**c**,**f**,**g**) of the figure were prepared with PyMOL, version 1.7.0.3 [20].

Despite this similarity, the binding of heparin to CK2α′ differs from its binding to CK2α in two key points, which appear to be correlated with each other:

- As illustrated by the comparative 2D plots in Figure 5d (CK2α′^{Cys336Ser}) and Figure 5e (CK2α$^{1-335}$), the orientation of the oligosaccharide chain is exactly reversed. This difference is also reflected in the fact that the bound heparin fragments hardly overlap (Figure 5c). In CK2α′^{Cys336Ser}, dp10 is exclusively in contact with the C-terminal domain of the enzyme, whereas in CK2α$^{1-335}$, parts of the N-terminal domain (e.g., Tyr50 from the ATP-binding loop; Figure 5e) contribute to dp10 binding.
- On the protein side, the heparin complex structures of CK2α$^{1-335}$ and CK2α′^{Cys336Ser} differ in the local conformation of helix αD, which follows the interdomain hinge region (Figure 5g). In CK2α′^{Cys336Ser}, this helix is not involved in heparin-binding, but in CK2α$^{1-335}$, it contributes to this via Lys122, which is in direct contact with two sulfo groups of dp10 (Figure 5e/g). This role of Lys122 requires a particular conformation of the hinge/helix αD region, referred to as the "closed conformation" in the literature [47] because of its most characteristic feature: occupation of the αD pocket by the side chain of Phe121 (Figure 5g).

This closed hinge/helix αD has occasionally been found in CK2α structures [47] (including in this work, namely in the CK2α$^{1-335}$/C02 complex, as illustrated in Figure 4e). Remarkably, however, it has been never observed so far with CK2α′. This and the associated differences in heparin-binding could reflect inherent characteristics and specific adaptations of the two isoenzymes. In particular, they could explain the otherwise puzzling fact that CK2α and CK2α′ differ in their substrate specificities, as reported recently [3] on the basis of an analysis of the phosphosite database [50]. The additional positive charge introduced into the upstream heparin and substrate-binding region of CK2α by Lys122 fits well with the fact that CK2α substrates are significantly more acidic than CK2α′ substrates in the sequence region upstream of the phosphorylation site (P-1 to P-4).

As convincing as this interpretation is, it must nevertheless be qualified with a reservation based on an older comparative analysis of CK2α structures [47]. According to that study, the closed hinge/αD conformation is disfavored by large ligands in the ATP/GTP cavity that interact directly with the interdomain hinge region. A ligand of this type is the indenoindole 4w (Figure 5b). 4w forms two halogen bonds with the hinge region of CK2α′^{Cys336Ser} (Figure 5g), but it was absent when the CK2α$^{1-335}$/dp10 complex structure was determined [30]. In the presence of 4w, it might prevent the closed hinge/αD conformation by CK2α$^{1-335}$ and, consequently, prevent Lys122 from participating in heparin-binding.

Further structural investigations are required to reveal to which extent CK2α and CK2α' really differ in their propensity to adopt the closed helix αD conformation and, as a consequence, in the composition and selectivity of their upstream substrate- and heparin-binding region. If the differences indicated by the results described here are confirmed, they appear to provide an attractive basis for the development of isoenzyme-selective bisubstrate inhibitors.

3. Materials and Methods

3.1. Crystallization of CK2α′^{Cys336Ser} and CK2α$^{1-335}$ in Complex with Various Ligands

For all protein crystallization experiments of this study, the sitting drop variant of the vapor diffusion method was applied at 20 °C. For this purpose, standard Cryschem plates from Hampton Research (Aliso Viejo, CA, USA) were used. If not explicitly stated otherwise, chemicals were purchased from Sigma Aldrich (Taufkirchen, Germany).

CK2$\alpha'^{Cys336Ser}$ was prepared as reported previously [28]. The final protein solution had the following composition: 5.3 mg/mL CK2$\alpha'^{Cys336Ser}$, 500 mM NaCl, 25 mM Tris/HCl, pH 8.5. To produce crystals for crystallographic fragment screening, 19 parts of volume of this CK2$\alpha'^{Cys336Ser}$ solution were mixed with one part by volume of 20 mM CX-4945 in DMSO to a final composition of 5 mg/mL CK2$\alpha'^{Cys336Ser}$, 1 mM CX-4945, and 5% (*v*/*v*) DMSO. CX-4945 was supplied by Sigma-Aldrich Chemie GmbH, Taufkirchen, Germany. After pre-incubation on ice for 30 min, the CK2$\alpha'^{Cys336Ser}$/CX-4945 mixture was centrifuged at high speed to remove any precipitate. Alternatively, when CK2$\alpha'^{Cys336Ser}$ crystals were required to determine a complex structure with the heparin fragment dp10 (Figure 5a), all steps mentioned so far were equivalent; however, CX-4945 was replaced by 4w (Figure 5b), which had been synthesized according to Haidar et al. [48].

In the case of CK2$\alpha'^{Cys336Ser}$/CX-4945 crystallization, each well of the crystallization plate contained 700 µL of reservoir solution composed of 28% (*w*/*v*) PEG6000, 900 mM LiCl, 250 mM Tris/HCl, pH 8.5. Each sitting drop was prepared by mixing 4 µL of the previously prepared CK2$\alpha'^{Cys336Ser}$/CX-4945 solution with 2 µL of reservoir solution. The formation of protein crystals was induced by microseeding, and the crystals were further optimized by macroseeding, as described previously [37]. In this way, about 300 CK2$\alpha'^{Cys336Ser}$/CX-4945 crystals were prepared for the purpose of crystallographic fragment screening. It should be noted that, with 250 mM, the buffer concentration in the reservoir (and in the drop after equilibration) was significantly higher than in the established protocol for CK2$\alpha'^{Cys336Ser}$ crystallization, where 100 mM Tris/HCl is mentioned [28,37]. In this way, the CK2$\alpha'^{Cys336Ser}$/CX-4945 crystals should be protected against potential pH-shifts caused by pH-active fragments of the F2X-Entry screen during soaking [38]. The details of this soaking process at the HZB F2X-Facility in Berlin, Germany, [41] are described separately below.

The heparin decasaccharide dp10 (Figure 5a) was purchased from Dextra Laboratories, Reading, UK. Prior to soaking with dp10, the mother liquor of CK2$\alpha'^{Cys336Ser}$/4w crystals was adapted from 900 mM LiCl to 50 mM LiCl in a stepwise manner, while in parallel the PEG6000 concentration was increased to saturation in order to maintain crystal stability. CK2$\alpha'^{Cys336Ser}$/4w crystals prepared in this way were soaked for at least 24 h in 50 mM dp10, saturated PEG6000, 50 mM LiCl, and 250 mM Tris/HCl, pH 8.5. This soaking solution allowed direct flash-freezing of the CK2$\alpha'^{Cys336Ser}$/4w/dp10 crystals in liquid nitrogen.

For comparative co-crystallization studies with CK2α^{1-335}, the fragments C02, D02, and F02 (Table 1) were purchased from BLD Pharmatech GmbH, Reinbek, Germany. CK2α^{1-335} was prepared as described by Werner et al. [35]. Its final solution had the following composition: 5 mg/mL CK2α^{1-335}, 500 mM NaCl, 25 mM Tris/HCl, pH 8.5. In addition, three CX-4945/fragment solutions were produced consisting of 10% (*v*/*v*) DMSO, 5 mM

CX-4945 plus 1 M of either C02, D02, or F02. One part by volume of each CX-4945/fragment solution was mixed with nine parts by volume of the purified CK2$\alpha^{1\text{-}335}$ solution. After pre-incubation on ice for 30 min, each of the CK2$\alpha^{1\text{-}335}$/CX-4945/fragment mixtures was centrifuged at high speed to remove any precipitates.

For CK2$\alpha^{1\text{-}335}$ crystallization, each well of the sitting drop crystallization plate contained 700 µL of reservoir solution composed of 35%-(*w*/*v*) PEG3350, 200 mM Li_2SO_4, 100 mM Bis-Tris/HCl, pH 6.5. The crystallization drops were mixtures of 2 µL reservoir solution and 4 µL pre-incubated CK2$\alpha^{1\text{-}335}$/CX-4945/fragment solution. Crystal growth was induced by microseeding. The final CK2$\alpha^{1\text{-}335}$/CX-4945/fragment crystals were shortly soaked in a mixture of one part by volume 30% (*v*/*v*) ethylene glycol (cryoprotectant) and nine parts by volume of reservoir solution and were subsequently flash-frozen in liquid nitrogen.

3.2. Soaking of CK2α′^{Cys336Ser}/CX-4945 Crystals with F2X-Entry Screen Fragments

The soaking of CK2α′^{Cys336Ser}/CX-4945 crystals with fragments of the F2X-Entry screen [38] was performed at the HZB F2X-Facility in Berlin, Germany [41]. MRC-3 96-well three-lens low-profile plates (JenaBioscience, Jena, Germany) were used, prepared with the potential ligands in dried form. Two of the three lenses belonging to one well contained the same fragment in an amount leading to a concentration of 100 mM after addition of 0.4 µL soaking solution.

Each lens with fragment powder, plus 30 further lenses without any fragment were filled with 0.4 µL soaking solution composed of 28%-(*w*/*v*) PEG6000, 900 mM LiCl, 250 mM Tris/HCl, pH 8.5, and 5%-(*v*/*v*) DMSO; afterwards, one CK2α′^{Cys336Ser}/CX-4945 crystal was added to each of the filled lenses. The rationale behind the fragment-free lenses was to provide electron densities of CK2α′^{Cys336Ser}/CX-4945 crystals that could serve as background correction in a sensitive search for ligands by "Pan-Dataset Density Analysis" (PanDDA) [46]. The reservoirs of the 96 wells were filled with 40 µL of a saturated PEG6000 solution in 900 mM LiCl, 250 mM Tris/HCl, pH 8.5, and 5% DMSO. The purpose of increasing the PEG6000 concentration to saturation was to combine the soaking step with dehydration of the crystals and thus achieve cryogenic conditions directly, without adding a special cryoprotectant. During preparation for soaking, the plate was covered with the EasyAccess Frame [51] to avoid evaporation of solvent during handling.

The CK2α′^{Cys336Ser}/CX-4945 crystals were soaked for 24 h at room temperature. Afterwards, they were harvested by flash-freezing in liquid nitrogen.

3.3. X-Ray Diffraction Data Collection and Processing

X-ray diffraction data from a total of 137 CK2α′^{Cys336Ser} crystals (two data sets per crystal) combined either with F2X-Entry screen fragments [38] or with fragment-free soaking solution were measured at beamline 14.1 of the HZB in Berlin (Germany) [52] at 100 K and a wavelength of 0.9184 Å. In each case, 1800 frames with 0.2° rotation were collected.

Further X-ray diffraction data were measured at beamline P13 of the EMBL outstation at DESY in Hamburg (Germany) [53] with CK2α′^{Cys336Ser}/4w/dp10 crystals as well as CK2$\alpha^{1\text{-}335}$/CX-4945/D02 crystals, and at beamline ID30B of the ESRF in Grenoble (France) [54] with CK2$\alpha^{1\text{-}335}$/C02 and CK2$\alpha^{1\text{-}335}$/CX-4945/F02 crystals.

All but two of the X-ray diffraction data sets were finally processed with autoPROC [55], which integrates XDS [56], Pointless and Aimless [57] from the CCP4 suite [58] and Staraniso [59]. The two exceptions were the diffraction data sets of the CK2α′^{Cys336Ser} crystals after soaking with fragment D04 and of the CK2$\alpha^{1\text{-}335}$/CX-4945/D02 crystals. In the first case, autoPROC [55] failed for unknown reasons, so that the standalone programs of the software pipeline had to be applied. In the latter case, the anisotropy analysis with

Staraniso [59] was left out because, in initial trials, it had provided poor statistics and led to very noisy electron density maps.

For those CK2α′^{Cys336Ser} and CK2α$^{1-335}$ structures submitted to the PDB [60], the essential details and statistics of the X-ray diffraction data are summarized in Table S1.

3.4. Structure Solution and Refinement

All structures of this study were determined by molecular replacement using Phaser [61], as implemented in Phenix [62], as the search program. The search model was either the CK2α′^{Cys336Ser} structure with PDB_ID 6HMQ [37] for the CK2α′^{Cys336Ser} structures or the CK2α$^{1-335}$ structure with PDB_ID 2PVR for the CK2α$^{1-335}$ structures.

The structures were refined with the phenix.refine module [63] of Phenix [62]. The bound ligands were parametrized with eLBOW [64]. Manual structure optimizations were performed with Coot [65]. The search for fragments in electron densities was perfomed in two rounds, first by manual inspection and second using PanDDA [46]. For Figures S1–S3, Fo-Fc OMIT maps [66,67] around the placed ligands were calculated using the corresponding Phenix routine [68]. Bulk solvent was excluded from omit regions, which is consistent with the rationale of polder maps [69]. Cartesian molecular dynamics including simulated annealing (starting temperature: 5000 K for structures with resolutions better than 1.5 Å and 3000 K for structures with resolutions worse than 1.5 Å) was applied to remove the memory of the structure for the respective ligand.

In case of the CK2α′^{Cys336Ser}/4w/dp10 structure, SGN and IDS residues of dp10 were added with Coot [65], and the carbohydrate chain as a whole was validated with Privateer [70].

4. Conclusions

Ten years ago, fragment screening with crystals of CK2α led to the discovery of the αD pocket [22], paving the way for a growing variety of bivalent CK2 inhibitors [19,22–27]. In this study, crystallographic fragment screening with human CK2α′, the isoenzyme of CK2α, and an established collection of pharmacologically interesting molecular fragments [38] is described. Although no completely new binding sites were discovered, a wealth of fragments previously unknown as ligands of CK2α or CK2α′ were identified (Table 1). Some of them have sufficiently high-affinity to the canonical ATP/GTP cavity to displace the tight-binding inhibitor CX-4945 [8], which was bound to the CK2α′ crystals used for fragment soaking, from this site under the soaking conditions.

Three of the fragments were found at the αD pocket (Figure 4), one of which (C02)—as revealed by a comparative crystallographic analysis with CK2α—binds exclusively to CK2α′. Linking this fragment chemically to a CK2α′-biased ATP/GTP-competitive inhibitor—as described, for example, by Lindenblatt et al. [37] or recently by Mudaliar et al. [36]—could potentially generate a bivalent inhibitor with even higher selectivity for CK2α′ over CK2α, which could be applied as a chemical tool for determining specific cellular functions of CK2α′ or lead to drugs for the treatment of CK2α′-associated pathologies such as Huntington's disease [71,72].

Five fragments were discovered as ligands at the interface to the regulatory subunit CK2β (Figure 3) and could potentially be used for the further development of the increasing number of CK2β-antagonistic compounds [13–18]. Since the affinities of CK2α and CK2α′ towards CK2β and CK2β antagonists such as cpd. 12 (Figures 1a and 3b–f) differ significantly [73], it is possible that fragments binding to the CK2β interface, like certain αD pocket ligands, can be exploited to generate bivalent CK2 inhibitors that can distinguish between CK2α and CK2α′.

Finally, crystallographic fragment screening paved the way to a CK2α′ crystal structure in complex with the decameric heparin fragment dp10 (Figure 5c), which is, to our knowledge, the first CK2α′ structure with a substrate-competitive inhibitor at all. A systematic comparison of this structure with a previously published CK2α/dp10 structure [30] revealed surprisingly large deviations both in the bound heparin fragments and in the enzyme matrices. Future studies will have to show whether these differences can lead to a next generation of isoenzyme-selective bisubstrate inhibitors.

Supplementary Materials: The following supporting information can be downloaded at: https://www.mdpi.com/article/10.3390/kinasesphosphatases4010001/s1, Table S1: Overview of PDB_IDs, protein crystallization, X-ray diffraction data collection, and structure refinement of all CK2α′^{Cys336Ser} and CK2α$^{1-335}$ structures resulting from this study; Figure S1: Alternative version of Figure 2 with Fo-Fc OMIT maps instead of 2Fo-Fc electron density maps; Figure S2: Alternative version of Figure 3 with Fo-Fc OMIT maps instead of 2Fo-Fc electron density maps; Figure S3: Alternative version of Figure 4 with Fo-Fc OMIT maps instead of 2Fo-Fc electron density maps.

Author Contributions: Conceptualization, C.W. and K.N.; methodology and investigation, C.W., T.B., H.H., C.M., M.S.W., M.L.B., and K.N.; validation, C.W. and K.N.; data curation, C.W. and K.N.; visualization, C.W. and K.N.; writing—original draft preparation, C.W. and K.N.; writing—review and editing, C.W., T.B., H.H., C.M., M.S.W., M.L.B., and K.N.; supervision, K.N.; project administration, K.N.; funding acquisition, K.N. and M.L.B. All authors have read and agreed to the published version of the manuscript.

Funding: This research was funded by the Deutsche Forschungsgemeinschaft (DFG), grant no. NI 643/11-1, and by the Agence Nationale de la Recherche (ANR), grant no. ANR-22-CE92-0081-01.

Institutional Review Board Statement: Not applicable.

Informed Consent Statement: Not applicable.

Data Availability Statement: The PDB identifiers of the CK2α′^{Cys336Ser} and CK2α$^{1-335}$ structures determined in this study are listed in the Supplementary Table S1. The DOI of the X-ray diffraction data collected at the ESRF is https://doi.org/10.15151/ESRF-ES-1897083444.

Acknowledgments: The authors thank Ulrich Baumann, University of Cologne, for access to the Cologne crystallization facility, which was installed with the support of the German Research Foundation (DFG) (grant number INST 216/682-1 FUGG). They are also grateful to the staff at HZB/BESSY, the ESRF, and the EMBL outstation at DESY, who enabled and supported the measurement of diffraction data at beamlines 14.1 (HZB/BESSY), ID30B (ESRF), and P13 (EMBL/DESY). C.M. and M.L.B. are indebted to the "Institut Convergence PLAsCAN" (ANR-17-CONV-0002) for supporting the project. C.W. would like to express his special thanks to Svenja Meyer for her help in preparing proteins and optimizing protein crystals as part of her studies for a Master's degree in Biochemistry at the University of Cologne.

Conflicts of Interest: The authors declare no conflicts of interest.

References

1. Kannan, N.; Neuwald, A.F. Evolutionary constraints associated with functional specificity of the CMGC protein kinases MAPK, CDK, GSK, SRPK, DYRK, and CK2α. *Protein Sci.* **2004**, *13*, 2059–2077. [CrossRef]
2. Niefind, K.; Guerra, B.; Ermakowa, I.; Issinger, O. Crystal structure of human protein kinase CK2: Insights into basic properties of the CK2 holoenzyme. *EMBO J.* **2001**, *20*, 5320–5331. [CrossRef]
3. Montenarh, M.; Götz, C. Protein Kinase CK2α′, More than a Backup of CK2α. *Cells* **2023**, *12*, 2834. [CrossRef] [PubMed]
4. Mayer, J.; Pack, M.; Montenarh, M.; Götz, C. Gene expression changes in pancreatic α-cell lines following knock-out of either CK2α or CK2α′. *Biol. Res.* **2025**, *58*, 69. [CrossRef] [PubMed]
5. Cozza, G.; A Pinna, L.; Moro, S. Protein kinase CK2 inhibitors: A patent review. *Expert Opin. Ther. Patents* **2012**, *22*, 1081–1097. [CrossRef] [PubMed]

6. Day-Riley, S.; West, R.M.; Brear, P.D.; Hyvönen, M.; Spring, D.R. CK2 Inhibitors Targeting Inside and Outside the Catalytic Box. *Kinases Phosphatases* **2024**, *2*, 110–135. [CrossRef]
7. Chen, Y.; Wang, Y.; Wang, J.; Zhou, Z.; Cao, S.; Zhang, J. Zhang, Strategies of Targeting CK2 in Drug Discovery: Challenges, Opportunities, and Emerging Prospects. *J. Med. Chem.* **2023**, *66*, 2257–2281. [CrossRef]
8. Siddiqui-Jain, A.; Drygin, D.; Streiner, N.; Chua, P.; Pierre, F.; O'Brien, S.E.; Bliesath, J.; Omori, M.; Huser, N.; Ho, C.; et al. CX-4945, an orally bioavailable selective inhibitor of protein kinase CK2, inhibits prosurvival and angiogenic signaling and exhibits antitumor efficacy. *Cancer Res.* **2010**, *70*, 10288–10298. [CrossRef]
9. Wells, C.I.; Drewry, D.H.; Pickett, J.E.; Tjaden, A.; Krämer, A.; Müller, S.; Gyenis, L.; Menyhart, D.; Litchfield, D.W.; Knapp, S.; et al. Development of a potent and selective chemical probe for the pleiotropic kinase CK2. *Cell Chem. Biol.* **2021**, *28*, 546–558.e10. [CrossRef]
10. Becher, I.; Savitski, M.F.; Hopf, C.; Bantscheff, M.; Drewes, G. Affinity profiling of the cellular kinome for the nucleotide cofactors ATP, ADP, and GTP. *ACS Chem. Biol.* **2013**, *8*, 599–607. [CrossRef]
11. Prudent, R.; Cochet, C. New protein kinase CK2 inhibitors: Jumping out of the catalytic box. *Chem. Biol.* **2009**, *16*, 112–120. [CrossRef]
12. Gower, C.M.; Chang, M.E.; Maly, D.J. Bivalent inhibitors of protein kinases. *Crit. Rev. Biochem. Mol. Biol.* **2014**, *49*, 102–115. [CrossRef] [PubMed]
13. Laudet, B.; Barette, C.; Dulery, V.; Renaudet, O.; Dumy, P.; Metz, A.; Prudent, R.; Deshiere, A.; Dideberg, O.; Filhol, O.; et al. Structure-based design of small peptide inhibitors of protein kinase CK2 subunit interaction. *Biochem. J.* **2007**, *408*, 363–373. [CrossRef] [PubMed]
14. Brear, P.; North, A.; Iegre, J.; Georgiou, K.H.; Lubin, A.; Carro, L.; Green, W.; Sore, H.F.; Hyvönen, M.; Spring, D.R. Novel non-ATP competitive small molecules targeting the CK2 α/β interface. *Bioorganic Med. Chem.* **2018**, *26*, 3016–3020. [CrossRef] [PubMed]
15. Kufareva, I.; Bestgen, B.; Brear, P.; Prudent, R.; Laudet, B.; Moucadel, V.; Ettaoussi, M.; Sautel, C.F.; Krimm, I.; Engel, M.; et al. Discovery of holoenzyme-disrupting chemicals as substrate-selective CK2 inhibitors. *Sci. Rep.* **2019**, *9*, 15893. [CrossRef]
16. Lindenblatt, D.; Horn, M.; Götz, C.; Niefind, K.; Neundorf, I.; Pietsch, M. Design of CK2β-Mimicking Peptides as Tools To Study the CK2α/CK2β Interaction in Cancer Cells. *ChemMedChem* **2019**, *14*, 833–841. [CrossRef]
17. Atkinson, E.L.; Iegre, J.; D'Amore, C.; Brear, P.; Salvi, M.; Hyvönen, M.; Spring, D.R. Development of small cyclic peptides targeting the CK2α/β interface. *Chem. Commun.* **2022**, *58*, 4791–4794. [CrossRef]
18. Raaf, J.; Guerra, B.; Neundorf, I.; Bopp, B.; Issinger, O.-G.; Jose, J.; Pietsch, M.; Niefind, K. First structure of protein kinase CK2 catalytic subunit with an effective CK2β-competitive ligand. *ACS Chem. Biol.* **2013**, *8*, 901–907. [CrossRef]
19. Lindenblatt, D.; Applegate, V.; Nickelsen, A.; Klußmann, M.; Neundorf, I.; Götz, C.; Jose, J.; Niefind, K. Molecular Plasticity of Crystalline CK2α′ Leads to KN2, a Bivalent Inhibitor of Protein Kinase CK2 with Extraordinary Selectivity. *J. Med. Chem.* **2022**, *65*, 1302–1312. [CrossRef]
20. *The PyMOL Molecular Graphics System*, Version 1.7.0.3; Schrödinger, LLC: New York, NY, USA, 2013.
21. Cimermancic, P.; Weinkam, P.; Rettenmaier, T.J.; Bichmann, L.; Keedy, D.A.; Woldeyes, R.A.; Schneidman-Duhovny, D.; Demerdash, O.N.; Mitchell, J.C.; Wells, J.A.; et al. CryptoSite: Expanding the Druggable Proteome by Characterization and Prediction of Cryptic Binding Sites. *J. Mol. Biol.* **2016**, *428*, 709–719. [CrossRef]
22. Brear, P.; De Fusco, C.; Georgiou, K.H.; Francis-Newton, N.J.; Stubbs, C.J.; Sore, H.F.; Venkitaraman, A.R.; Abell, C.; Spring, D.R.; Hyvönen, M. Specific inhibition of CK2α from an anchor outside the active site. *Chem. Sci.* **2016**, *7*, 6839–6845. [CrossRef]
23. De Fusco, C.; Brear, P.; Iegre, J.; Georgiou, K.H.; Sore, H.F.; Hyvönen, M.; Spring, D.R. A fragment-based approach leading to the discovery of a novel binding site and the selective CK2 inhibitor CAM4066. *Bioorganic Med. Chem.* **2017**, *25*, 3471–3482. [CrossRef]
24. Glossop, P.A.; Brear, P.; Wright, S.; Flanagan, N.; Glossop, M.S.; Lane, C.A.L.; Butt, R.P.; Spring, D.R.; Hyvönen, M.; Cawkill, D. Exploiting the Cryptic αD Pocket of Casein Kinase 2α (CK2α) to Deliver Highly Potent and Selective Type 1 Inhibitors. *J. Med. Chem.* **2025**, *68*, 21587–21614. [CrossRef]
25. Marlhoux, L.; Arnaud, A.; Hervieu, C.; Makulyte, G.; Martinasso, C.; Mularoni, A.; Delcros, J.-G.; Krimm, I.; Hernandez-Vargas, H.; Ichim, G.; et al. Discovery of KDX1381, a Bivalent CK2α Inhibitor for the Treatment of Solid Tumors as a Single Agent or in Combination. *J. Med. Chem.* **2025**, *68*, 12819–12844. [CrossRef] [PubMed]
26. Grenier, D.; Molina, D.S.L.; Gelin, M.; Mularoni, A.; Guichou, J.-F.; Delcros, J.-G.; Martinasso, C.; Yang, Y.; Ahnou, N.; Pawlotsky, J.-M.; et al. Picomolar bivalent inhibitors of protein kinase CK2 active against β-coronavirus replication. *Eur. J. Med. Chem.* **2025**, *296*, 117826. [CrossRef] [PubMed]
27. Bancet, A.; Frem, R.; Jeanneret, F.; Mularoni, A.; Bazelle, P.; Roelants, C.; Delcros, J.-G.; Guichou, J.-F.; Pillet, C.; Coste, I.; et al. Cancer selective cell death induction by a bivalent CK2 inhibitor targeting the ATP site and the allosteric αD pocket. *iScience* **2024**, *27*, 108903. [CrossRef]

28. Werner, C.; Lindenblatt, D.; Viht, K.; Uri, A.; Niefind, K. Discovery and Exploration of Protein Kinase CK2 Binding Sites Using CK2$\alpha'^{Cys336Ser}$ as an Exquisite Crystallographic Tool. *Kinases Phosphatases* **2023**, *1*, 306–322. [CrossRef]
29. O'Farrell, F.; Loog, M.; Janson, I.M.; Ek, P. Kinetic study of the inhibition of CK2 by heparin fragments of different length. *Biochim. Biophys. Acta BBA-Protein Struct. Mol. Enzym.* **1999**, *1433*, 68–75. [CrossRef]
30. Schnitzler, A.; Niefind, K. Structural basis for the design of bisubstrate inhibitors of protein kinase CK2 provided by complex structures with the substrate-competitive inhibitor heparin. *Eur. J. Med. Chem.* **2021**, *214*, 113223. [CrossRef]
31. Hathaway, G.; Lubben, T.; Traugh, J.A. Inhibition of casein kinase II by heparin. *J. Biol. Chem.* **1980**, *255*, 8038–8041. [CrossRef]
32. Mäenpää, P.H. Effects of polyamines and polyanions on a cyclic nucleotide-independent and a cyclic AMP-dependent protein kinase. *Biochim. Biophys. Acta* **1977**, *498*, 294–305. [CrossRef] [PubMed]
33. Meggio, F.; Pinna, L.A. One-thousand-and-one substrates of protein kinase CK2? *FASEB J.* **2003**, *17*, 349–368. [CrossRef]
34. Turowec, J.P.; Vilk, G.; Gabriel, M.; Litchfield, D.W. Characterizing the convergence of protein kinase CK2 and caspase-3 reveals isoform-specific phosphorylation of caspase-3 by CK2α′: Implications for pathological roles of CK2 in promoting cancer cell survival. *Oncotarget* **2013**, *4*, 560–571. [CrossRef] [PubMed]
35. Werner, C.; Gast, A.; Lindenblatt, D.; Nickelsen, A.; Niefind, K.; Jose, J.; Hochscherf, J. Structural and Enzymological Evidence for an Altered Substrate Specificity in Okur-Chung Neurodevelopmental Syndrome Mutant CK2α. *Front. Mol. Biosci.* **2022**, *9*, 831693. [CrossRef]
36. Mudaliar, D.; Mansky, R.H.; White, A.; Baudhuin, G.; Hawkinson, J.; Wong, H.; Walters, M.A.; Gomez-Pastor, R. Discovery of a CK2α′-Biased ATP-Competitive Inhibitor from a High-Throughput Screen of an Allosteric-Inhibitor-Like Compound Library. *ACS Chem. Neurosci.* **2024**, *15*, 2703–2718. [CrossRef]
37. Lindenblatt, D.; Nickelsen, A.; Applegate, V.M.; Hochscherf, J.; Witulski, B.; Bouaziz, Z.; Marminon, C.; Bretner, M.; Le Borgne, M.; Jose, J.; et al. Diacritic binding of an indenoindole inhibitor by CK2α paralogs explored by a reliable path to atomic resolution CK2α′ structures. *ACS Omega* **2019**, *4*, 5471–5478. [CrossRef] [PubMed]
38. Wollenhaupt, J.; Metz, A.; Barthel, T.; Lima, G.M.; Heine, A.; Mueller, U.; Klebe, G.; Weiss, M.S. F2X-Universal and F2X-Entry: Structurally Diverse Compound Libraries for Crystallographic Fragment Screening. *Structure* **2020**, *28*, 694–706.e5. [CrossRef]
39. Wollenhaupt, J.; Barthel, T.; Lima, G.; Metz, A.; Wallacher, D.; Jagudin, E.; Huschmann, F.U.; Hauß, T.; Feiler, C.G.; Gerlach, M. Workflow and Tools for Crystallographic Fragment Screening at the Helmholtz-Zentrum Berlin. *J. Vis. Exp.* **2021**, *169*, e62208. [CrossRef]
40. Metz, A.; Wollenhaupt, J.; Glöckner, S.; Messini, N.; Huber, S.; Barthel, T.; Merabet, A.; Gerber, H.-D.; Heine, A.; Klebe, G.; et al. Frag4Lead: Growing crystallographic fragment hits by catalog using fragment-guided template docking. *Acta Crystallogr. Sect. D Struct. Biol.* **2021**, *77*, 1168–1182. [CrossRef]
41. Barthel, T.; Benz, L.; Basler, Y.; Crosskey, T.; Dillmann, A.; Förster, R.; Fröling, P.; Dieguez, C.G.; Gless, C.; Hauß, T.; et al. The HZB F2X-Facility—An Efficient Crystallographic Fragment Screening Platform. *Appl. Res.* **2024**, *3*, e202400110. [CrossRef]
42. Battistutta, R.; Cozza, G.; Pierre, F.; Papinutto, E.; Lolli, G.; Sarno, S.; O'brien, S.E.; Siddiqui-Jain, A.; Haddach, M.; Anderes, K.; et al. Unprecedented selectivity and structural determinants of a new class of protein kinase CK2 inhibitors in clinical trials for the treatment of cancer. *Biochemistry* **2011**, *50*, 8478–8488. [CrossRef]
43. Tucker, J.K.; Da Silva, I.I.; Gage, F.H. Scaffold hopping and sidechain modification from a flavone scaffold lead to discovery of potent, selective CK2A2 inhibitors with favorable properties for CNS activity. *Bioorg. Med. Chem.* **2025**, *127*, 118196. [CrossRef]
44. Buchwald, L.M.; Neess, D.; Hansen, D.; Doktor, T.K.; Ramesh, V.; Steffensen, L.B.; Blagoev, B.; Litchfield, D.W.; Andresen, B.S.; Ravnskjaer, K.; et al. Body weight control via protein kinase CK2: Diet-induced obesity counteracted by pharmacological targeting. *Metabolism* **2025**, *162*, 156060. [CrossRef] [PubMed]
45. Raaf, J.; Bischoff, N.; Klopffleisch, K.; Brunstein, E.; Olsen, B.B.; Vilk, G.; Litchfield, D.W.; Issinger, O.-G.; Niefind, K. Interaction between CK2α and CK2β, the Subunits of Protein Kinase CK2: Thermodynamic Contributions of Key Residues on the CK2α Surface. *Biochemistry* **2011**, *50*, 512–522. [CrossRef] [PubMed]
46. Pearce, N.M.; Krojer, T.; Bradley, A.R.; Collins, P.; Nowak, R.P.; Talon, R.; Marsden, B.D.; Kelm, S.; Shi, J.; Deane, C.M.; et al. A multi-crystal method for extracting obscured crystallographic states from conventionally uninterpretable electron density. *Nat. Commun.* **2017**, *8*, 15123. [CrossRef]
47. Klopffleisch, K.; Issinger, O.-G.; Niefind, K. Niefind, Low-density crystal packing of human protein kinase CK2 catalytic subunit in complex with resorufin or other ligands: A tool to study the unique hinge-region plasticity of the enzyme without packing bias. *Acta Crystallogr. Sect. D Struct. Biol.* **2012**, *68*, 883–892. [CrossRef] [PubMed]
48. Haidar, S.; Marminon, C.; Aichele, D.; Nacereddine, A.; Zeinyeh, W.; Bouzina, A.; Berredjem, M.; Ettouati, L.; Bouaziz, Z.; Le Borgne, M.; et al. QSAR model of indeno [1,2-*b*]indole derivatives and identification of *N*-isopentyl-2-methyl-4,9-dioxo-4,9-dihydronaphtho[2,3-*b*]furan-3-carboxamide as a potent CK2 inhibitor. *Molecules* **2019**, *25*, 97. [CrossRef]

49. Laskowski, R.A.; Swindells, M.B. LigPlot+: Multiple ligand-protein interaction diagrams for drug discovery. *J. Chem. Inf. Model.* **2011**, *51*, 2778–2786. [CrossRef]
50. Hornbeck, P.V.; Kornhauser, J.M.; Latham, V.; Murray, B.; Nandhikonda, V.; Nord, A.; Skrzypek, E.; Wheeler, T.; Zhang, B.; Gnad, F. 15 years of PhosphoSitePlus®: Integrating post-translationally modified sites, disease variants and isoforms. *Nucleic Acids Res.* **2019**, *47*, D433–D441. [CrossRef]
51. Barthel, T.; Huschmann, F.U.; Wallacher, D.; Feiler, C.G.; Klebe, G.; Weiss, M.S.; Wollenhaupt, J. Facilitated crystal handling using a simple device for evaporation reduction in microtiter plates. *J. Appl. Crystallogr.* **2021**, *54*, 376–382. [CrossRef]
52. Mueller, U.; Barthel, T.; Benz, L.S.; Bon, V.; Crosskey, T.; Dieguez, C.G.; Förster, R.; Gless, C.; Hauß, T.; Heinemann, U.; et al. The macromolecular crystallography beamlines of the Helmholtz-Zentrum Berlin at the BESSY II storage ring: History, current status and future directions. *J. Synchrotron Radiat.* **2025**, *32*, 766–778. [CrossRef]
53. Cianci, M.; Bourenkov, G.; Pompidor, G.; Karpics, I.; Kallio, J.; Bento, I.; Roessle, M.; Cipriani, F.; Fiedler, S.; Schneider, T.R. P13, the EMBL macromolecular crystallography beamline at the low-emittance PETRA III ring for high- and low-energy phasing with variable beam focusing. *J. Synchrotron Radiat.* **2017**, *24*, 323–332. [CrossRef]
54. McCarthy, A.A.; Barrett, R.; Beteva, A.; Caserotto, H.; Dobias, F.; Felisaz, F.; Giraud, T.; Guijarro, M.; Janocha, R.; Khadrouche, A.; et al. ID30B—A versatile beamline for macromolecular crystallography experiments at the ESRF. *J. Synchrotron. Radiat.* **2018**, *25*, 1249–1260. [CrossRef] [PubMed]
55. Vonrhein, C.; Flensburg, C.; Keller, P.; Sharff, A.; Smart, O.; Paciorek, W.; Womack, T.; Bricogne, G. Data processing and analysis with the autoPROC toolbox. *Acta Crystallogr. D Biol. Crystallogr.* **2011**, *67*, 293–302. [CrossRef] [PubMed]
56. Kabsch, W. XDS. *Acta Crystallogr. D Biol. Crystallogr.* **2010**, *66*, 125–132. [CrossRef]
57. Evans, P.R.; Murshudov, G.N. How good are my data and what is the resolution? *Acta Crystallogr. D Biol. Crystallogr.* **2013**, *69*, 1204–1214. [CrossRef] [PubMed]
58. Winn, M.D.; Ballard, C.C.; Cowtan, K.D.; Dodson, E.J.; Emsley, P.; Evans, P.R.; Keegan, R.M.; Krissinel, E.B.; Leslie, A.G.; McCoy, A.; et al. Overview of the CCP4 suite and current developments. *Acta Crystallogr. D Biol. Crystallogr.* **2011**, *67*, 235–242. [CrossRef]
59. Tickle, I.J.; Flensburg, C.; Keller, P.; Paciorek, W.; Sharff, A.; Vonrhein, C.; Bricogne, G. *STARANISO*; Global Phasing Ltd.: Cambridge, UK, 2018.
60. wwPDB Consortium. Protein Data Bank: The single global archive for 3D macromolecular structure data. *Nucleic Acids Res.* **2019**, *47*, D520–D528. [CrossRef]
61. McCoy, A.J.; Grosse-Kunstleve, R.W.; Adams, P.D.; Winn, M.D.; Storoni, L.C.; Read, R.J. Phaser crystallographic software. *J. Appl. Crystallogr.* **2007**, *40*, 658–674. [CrossRef]
62. Adams, P.D.; Afonine, P.V.; Bunkóczi, G.; Chen, V.B.; Davis, I.W.; Echols, N.; Headd, J.J.; Hung, L.W.; Kapral, G.J.; Grosse-Kunstleve, R.W.; et al. PHENIX: A comprehensive Python-based system for macromolecular structure solution. *Acta Crystallogr. D Biol. Crystallogr.* **2010**, *66*, 213–221. [CrossRef]
63. Afonine, P.V.; Grosse-Kunstleve, R.W.; Echols, N.; Headd, J.J.; Moriarty, N.W.; Mustyakimov, M.; Terwilliger, T.C.; Urzhumtsev, A.; Zwart, P.H.; Adams, P.D. Towards automated crystallographic structure refinement with *phenix.refine*. *Acta Crystallogr. D Biol. Crystallogr.* **2012**, *68*, 352–367. [CrossRef] [PubMed]
64. Moriarty, N.W.; Grosse-Kunstleve, R.W.; Adams, P.D. Electronic Ligand Builder and Optimization Workbench (eLBOW): A tool for ligand coordinate and restraint generation. *Acta Crystallogr. D Biol. Crystallogr.* **2009**, *65*, 1074–1080. [CrossRef] [PubMed]
65. Emsley, P.; Lohkamp, B.; Scott, W.G.; Cowtan, K. Features and development of Coot. *Acta Crystallogr. D Biol. Crystallogr.* **2010**, *66*, 486–501. [CrossRef]
66. Bhat, T.N. Calculation of an OMIT map. *J. Appl. Cryst.* **1988**, *21*, 279–281. [CrossRef]
67. Hodel, A.; Kim, S.H.; Brünger, A.T. Model bias in macromolecular crystal structures. *Acta Cryst.* **1992**, *A48*, 851–858. [CrossRef]
68. Terwilliger, T.C.; Grosse-Kunstleve, R.W.; Afonine, P.V.; Moriarty, N.W.; Adams, P.D.; Read, R.J.; Zwart, P.H.; Hung, L.W. Iterative-build OMIT maps: Map improvement by iterative model building and refinement without model bias. *Acta Crystallogr. D Biol. Crystallogr.* **2008**, *64*, 515–524. [CrossRef]
69. Liebschner, D.; Afonine, P.V.; Moriarty, N.W.; Poon, B.K.; Sobolev, O.V.; Terwilliger, T.C.; Adams, P.D. Polder maps: Improving OMIT maps by excluding bulk solvent. *Acta Crystallogr. D Struct. Biol.* **2017**, *73*, 148–157. [CrossRef]
70. Agirre, J.; Iglesias-Fernández, J.; Rovira, C.; Davies, G.J.; Wilson, K.S.; Cowtan, K.D. Privateer: Software for the conformational validation of carbohydrate structures. *Nat. Struct. Mol. Biol.* **2015**, *22*, 833–834. [CrossRef]
71. Yu, D.; Zarate, N.; White, A.; Coates, D.J.; Tsai, W.; Nanclares, C.; Cuccu, F.; Yue, J.S.; Brown, T.G.; Mansky, R.H.; et al. CK2 alpha prime and alpha-synuclein pathogenic functional interaction mediates synaptic dysregulation in Huntington's disease. *Acta Neuropathol. Commun.* **2022**, *10*, 83. [CrossRef]

72. Gomez-Pastor, R.; Burchfiel, E.T.; Neef, D.W.; Jaeger, A.M.; Cabiscol, E.; McKinstry, S.U.; Doss, A.; Aballay, A.; Lo, D.C.; Akimov, S.S.; et al. Thiele, Abnormal degradation of the neuronal stress-protective transcription factor HSF1 in Huntington's disease. *Nat. Commun.* **2017**, *8*, 14405. [CrossRef] [PubMed]
73. Werner, C.; Eimermacher, S.; Harasimowicz, H.; Fischer, D.; Pietsch, M.; Niefind, K. A CK2α′ mutant indicating why CK2α and CK2α′, the isoforms of the catalytic subunit of human protein kinase CK2, deviate in affinity to CK2β. *Biol. Chem.* **2025**, *406*, 101–115. [CrossRef] [PubMed]